Benzene–Pyridine Interactions Predicted by the Effective Fragment Potential Method

ARTICLE *in* THE JOURNAL OF PHYSICAL CHEMISTRY A · MAY 2011

Impact Factor: 2.69 · DOI: 10.1021/jp201039b · Source: PubMed

3 AUTHORS, INCLUDING:

Lyudmila Slipchenko
Purdue University
63 PUBLICATIONS **3,278** CITATIONS

SEE PROFILE

THE JOURNAL OF PHYSICAL CHEMISTRY A

ARTICLE

pubs.acs.org/JPCA

Benzene−Pyridine Interactions Predicted by the Effective Fragment Potential Method

Quentin A. Smith and Mark S. Gordon*

Department of Chemistry, Iowa State University, Ames, Iowa 50011, United States

Lyudmila V. Slipchenko

Department of Chemistry, Purdue University, West Lafayette, Indiana 47907, United States

Supporting Information

ABSTRACT: The accurate representation of nitrogen-containing heterocycles is essential for modeling biological systems. In this study, the general effective fragment potential (EFP2) method is used to model dimers of benzene and pyridine, complexes for which high-level theoretical data —including large basis spin-component-scaled second-order perturbation theory (SCS-MP2), symmetry-adapted perturbation theory (SAPT), and coupled cluster with singles, doubles, and perturbative triples (CCSD(T))—are available. An extensive comparison of potential energy curves and components of the interaction energy is presented for sandwich, T-shaped, parallel displaced, and hydrogen-bonded structures of these dimers. EFP2 and CCSD(T) potential energy curves for the sandwich, T-shaped, and hydrogen-bonded dimers have an average root-mean-square deviation (RMSD) of 0.49 kcal/mol; EFP2 and SCS-MP2 curves for the parallel displaced dimers have an average RMSD of 0.52 kcal/mol. Additionally, results are presented from an EFP2 Monte Carlo/simulated annealing (MC/SA) computation to sample the potential energy surface of the benzene−pyridine and pyridine dimers.

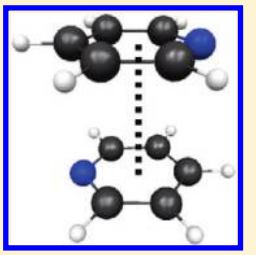

INTRODUCTION

Aromatic $\pi-\pi$ interactions are of fundamental importance in biological systems: they appear in protein folding,[1] DNA structure,[2] and drug binding.[3] Benzene and substituted benzene dimers have been used as model systems to study these interactions, but biologically important molecules, including amino acids and DNA bases, often contain aromatic heterocycles in addition to substituents on the aromatic ring. Therefore, for a theoretical method to be useful for modeling biological systems, it must be able to accurately describe the effects on $\pi-\pi$ interactions arising from both ring substituents and from heteroatom (especially nitrogen) substitution.

The general effective fragment potential (EFP2)[4] method has previously been used to model the $\pi-\pi$ and $\pi-$hydrogen interactions of benzene dimers,[5] benzene−water complexes,[6] and substituted benzene dimers[7] to a high degree of accuracy, approaching that of coupled cluster theory with singles, doubles, and perturbative triples (CCSD(T)).[8] The present work extends these benchmark EFP2 studies to examine the $\pi-\pi$ and $\pi-$hydrogen interactions of aromatic nitrogen-containing heterocycles, specifically dimers of pyridine and benzene−pyridine. Pyridine and benzene−pyridine interactions have been examined extensively at a high level of ab initio theory by Hohenstein and Sherrill.[9] Also notable are previous density functional theory (DFT)[10] and combined ab initio and DFT investigations.[11] A favorable comparison between EFP2 and the high-level results for these chemical systems will help to establish EFP2 as a viable method for modeling more complex biomolecules.

EFP2 is an ab initio-based model potential method that was designed to model intermolecular interactions. A set of parameters to account for the major noncovalent forces—Coulomb, exchange-repulsion, polarization (induction), and dispersion—for each unique fragment is derived from a single ab initio calculation. These parameters can be used in subsequent calculations to model interactions with other EFP fragments or with ab initio molecules. Unlike many other model potential methods, the parameters are not empirically fitted. EFP fragments have frozen internal geometries.

The advantage of EFP over traditional ab inito methods is its low computational cost. For example, a single-point energy calculation for the benzene dimer with second-order perturbation theory (MP2)[12] and the 6-311++G(3df,2p) basis set[13] takes 142 min on a single IBM Power5 processor, while an EFP2 calculation with the same basis set takes only 0.4 s, after the EFP2 potential has been generated in a prior calculation.[5] The calculation to generate the EFP2 potential on a single fragment takes about as long as a MP2 calculation.

THEORETICAL METHODS

The general effective fragment potential (EFP2) method is coded in the GAMESS (General Atomic and Molecular Electronic Structure System)[14] computational chemistry software package, which was used for all calculations in this study. The EFP2

Received: January 31, 2011
Revised: March 24, 2011
Published: April 19, 2011

energy is comprised of Coulomb, exchange-repulsion, polarization (induction), dispersion, and charge transfer terms. The Coulomb term is computed via Stone's distributed multipolar expansion,[15] carried out through octopole moments. Both analytical and numerical[16] distributed multipolar analysis (DMA) is available; the numerical DMA was chosen for this study. Exchange-repulsion is derived as an expansion in the intermolecular overlap, truncated at the quadratic term.[17] EFP2 polarization is expressed as a sum of localized molecular orbital (LMO) polarizabilities, where the polarizable points are located at the LMO centroids (i.e., valence bonds and lone pairs of the molecule). The LMO polarizabilities are calculated from the coupled-perturbed Hartree−Fock equations. Dispersion is expressed as $E_{disp} \approx C_6/R^6 + C_8/R^8$, with an explicitly derived C_6/R^6 term and an estimated C_8/R^8 term. The C_6 coefficient is derived from the frequency-dependent polarizabilities integrated over the imaginary frequency range.[18] The charge transfer term, which is omitted in the present work, was derived using a perturbative analysis of the interaction between occupied orbitals on one fragment and virtual orbitals on a second fragment.[19] The charge transfer interaction is significant only if charged or highly polar species (e.g., water) are present; previous work[19] has shown that this term does not contribute significantly to the total interaction energy of most neutral molecules.

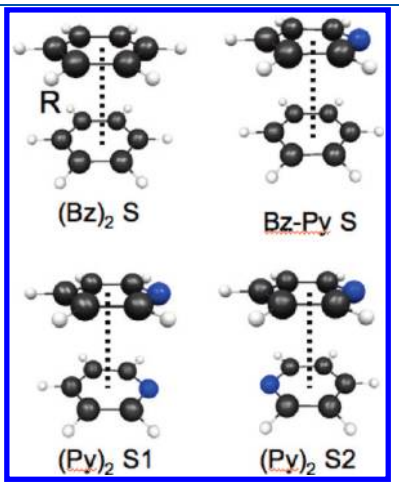

Figure 1. Sandwich configurations of benzene ($(Bz)_2$), benzene−pyridine (Bz−Py), and pyridine ($(Py)_2$) dimers. R is the distance between ring centers.

Various Coulomb damping functions are employed in the EFP2 method for modeling charge penetration.[20] In this study, charge penetration was modeled by an exponential damping function multiplying the distributed multipoles, including charge−charge, charge−dipole, charge−quadrupole, dipole−dipole, and dipole−quadrupole terms. The polarization and dispersion terms were also screened to account for close range interactions. Polarization screening takes the form of a Gaussian function, and dispersion screening uses an overlap-based damping factor, both with no parametrization. These damping functions are described extensively in ref 20.

Monomer and dimer geometries for benzene−pyridine and pyridine−pyridine dimers were obtained from ref 9. In that work, experimental geometries were chosen for the monomers. The monomer geometry of benzene is from Gauss and Stanton,[21] with a carbon−carbon bond length of 1.3915 Å and a carbon−hydrogen bond length of 1.0800 Å. The monomer geometry of pyridine is that of Innes et al.[22] EFP2 potentials for the monomers at these geometries were calculated with the 6-311++G(3df,2p) basis. In both ref 9 and in the present study, the monomers are held rigid, having fixed internal coordinates.

Dimer geometries were also obtained from ref 9. These geometries were chosen in order to gain a better understanding of fundamental $\pi-\pi$ and π−hydrogen interactions and to examine how these interactions are affected by the heteroatom; therefore, the dimer geometries are not potential energy minima or experimentally obtained structures. (For example, the benzene dimer sandwich structure is a saddle point between two symmetry-equivalent parallel displaced structures.[23]) Three major classes of benzene (Bz) and pyridine (Py) dimer geometries were examined: sandwich (Figure 1), T-shaped (Figure 2), and parallel displaced (Figure 3). For sandwich and T-shaped dimers, the distance R is a measure of the vertical separation between

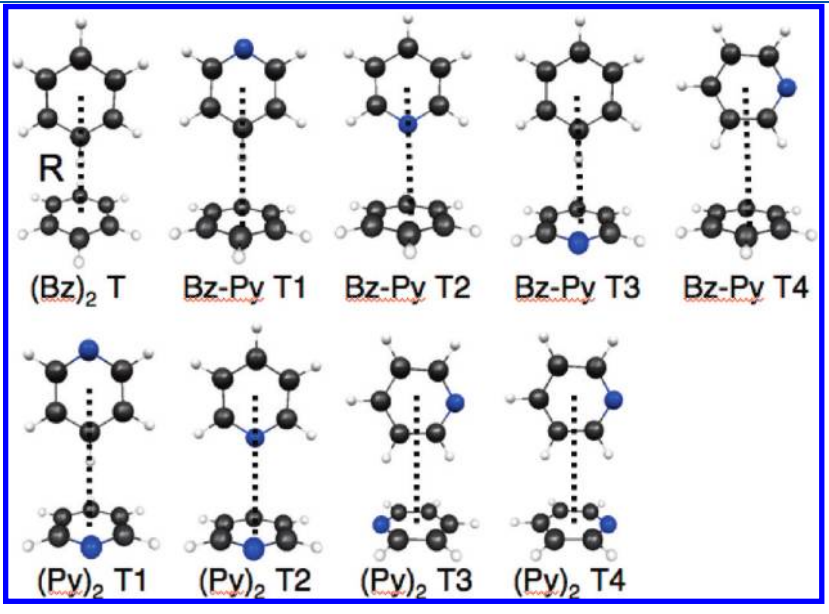

Figure 2. T-shaped configurations of benzene ($(Bz)_2$), benzene−pyridine (Bz−Py), and pyridine ($(Py)_2$) dimers. R is the distance between ring centers.

dx.doi.org/10.1021/jp201039b |J. Phys. Chem. A 2011, 115, 4598–4609

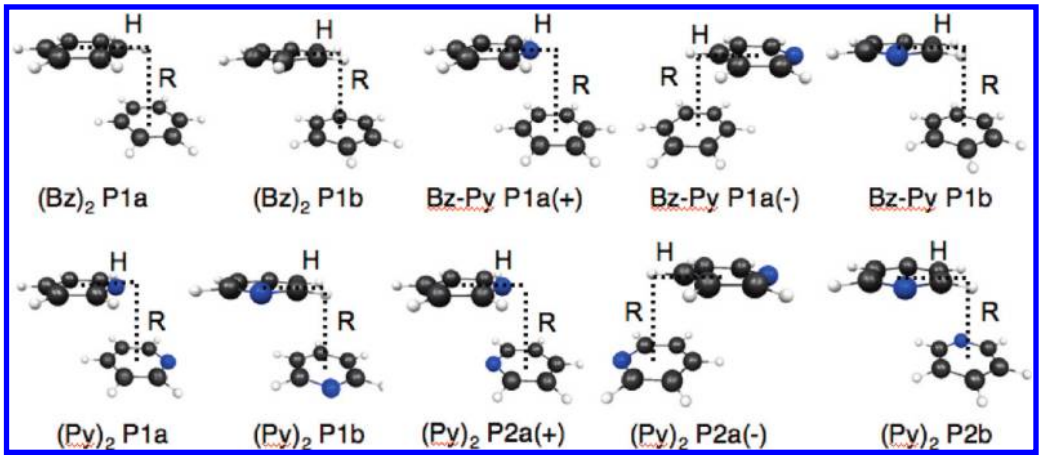

Figure 3. Parallel displaced configurations of benzene ($(Bz)_2$), benzene−pyridine (Bz−Py), and pyridine ($(Py)_2$) dimers. *R* is the vertical separation, and *H* is the horizontal separation between monomers.

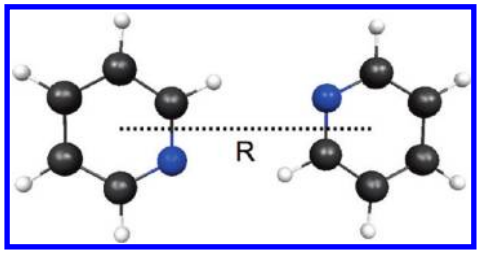

Figure 4. Configuration of the hydrogen-bonded pyridine dimer. *R* is the distance between ring centers.

the ring centers. Potential energy curves for these two types of dimers were obtained by varying *R* in increments of 0.1 Å near the potential minimum (3.2 Å ≤ *R* ≤ 5.0 Å for sandwich; 4.2 Å ≤ *R* ≤ 6.0 Å for T-shaped) and by 0.5 Å far from the minimum (5.0 Å ≤ *R* ≤ 7.0 Å for sandwich; 6.0 Å ≤ *R* ≤ 9.0 Å for T-shaped). Individual parallel displaced configurations had a vertical displacement *R* of 3.4 Å and a horizontal displacement *H* of 1.6 Å. These choices facilitate comparison with results from symmetry-adapted perturbation theory (see below). To generate parallel displaced potential energy curves, the vertical displacement was fixed at 3.5 Å, while the horizontal displacement was varied in increments of 0.2 Å. Parallel displaced conformations pass through sandwich conformations at *H* = 0 Å. They are designated with an "a" if the horizontal displacement goes over a vertex (the heteroatom), and they are designated with a "b" if the displacement goes over an edge (the bond between pyridine carbons 2 and 3). A (+) or a (−) indicates the direction of the displacement in cases in which the displacement is not symmetric. Displacement of the upper monomer is considered to be positive if it is moved left to right relative to the perspective shown in Figure 3.

Although the major focus of this study is on $\pi-\pi$ and π−hydrogen interactions, the hydrogen-bonded pyridine dimer was investigated as well (Figure 4), due to the importance of hydrogen-bonded interactions in biological compounds. The distance between ring centers, *R*, in the hydrogen- bonded complex was varied in increments of 0.1 Å.

EFP2 total interaction energies and potential energy curves are compared with those reported in ref 9. The calculations reported by Hohenstein and Sherrill[9] were performed as follows.

Table 1. Comparison of EFP2 and CCSD(T) Potential Energy Minima of Sandwich and T-Shaped Configurations of Benzene, Benzene−Pyridine, and Pyridine Dimers[a]

	CCSD(T) (ref 9)		EFP2	
	Δ*E*	*R*	Δ*E*	*R*
$(Bz)_2$ S	−1.76	3.9	−2.33	3.9
Bz−Py S	−2.22	3.8	−3.01	3.9
$(Py)_2$ S1	−1.61	3.8	−2.38	3.9
$(Py)_2$ S2	−2.95	3.7	−3.85	3.8
$(Bz)_2$ T	−2.73	5.0	−3.01	5.1
Bz−Py T1	−3.18	4.9	−3.34	5.2
Bz−Py T2*	−0.64	4.7	0.08	4.8
Bz−Py T3	−2.20	5.0	−2.53	5.0
Bz−Py T4	−2.74	5.0	−2.86	5.1
$(Py)_2$ T1	−2.46	5.0	−2.69	5.0
$(Py)_2$ T2*	−1.23	4.6	−0.45	4.8
$(Py)_2$ T3	−2.95	4.9	−2.92	5.1
$(Py)_2$ T4*	−2.15	5.0	−2.14	5.1

[a] Intermonomer separation (*R*, Å) and interaction energy (Δ*E*, kcal/mol) of potential minima of sandwich (S) and T-shaped (T) dimers. The CCSD(T) data, taken from ref 9 is estimated to the complete basis set (CBS) limit, except where noted by (*). The (*) dimers are est. CCSD(T)/aug-cc-pVTZ.

For the sandwich, T-shaped, and hydrogen-bonded dimers, large-basis CCSD(T) single-point energies were computed by adding a coupled-cluster correction to a large-basis second-order perturbation theory (MP2) energy: $E_{CCSD(T)}^{large\text{-}basis} \approx E_{MP2}^{large\text{-}basis} + \Delta CCSD(T)$. The correction, ΔCCSD(T), is the difference between a CCSD(T) energy and an MP2 energy obtained with a smaller basis: $\Delta CCSD(T) = E_{CCSD(T)}^{small\text{-}basis} - E_{MP2}^{small\text{-}basis}$. The MP2 complete basis set (CBS) limit was estimated using the aug-cc-pVTZ and aug-cc-pVQZ basis sets[24] with the two-point extrapolation scheme of Haliker et al.[25] Energies for the parallel displaced configurations were calculated using spin-component-scaled second-order perturbation theory (SCS-MP2)[26] with the aug-cc-pVTZ basis set. The Boys−Bernardi counterpoise correction[27] was employed to account for basis set superposition error (BSSE) with all energy computations. (Note that BSSE corrections are not required for the EFP2 method.)

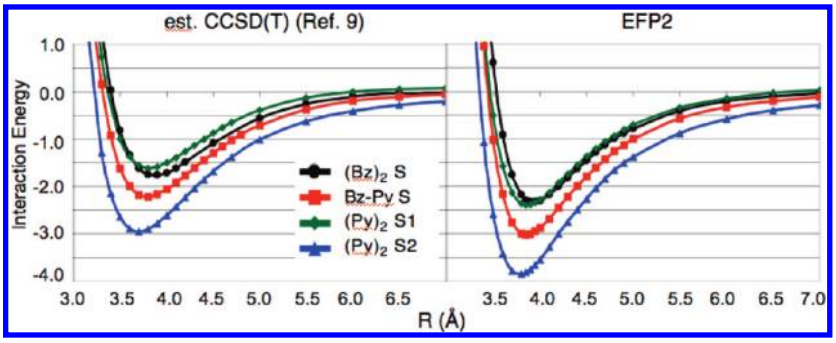

Figure 5. Est. CCSD(T)/CBS[9] (left) and EFP2 (right) potential energy curves for the sandwich configurations. Interaction energy is in kcal/mol.

To analyze contributions to the total interaction energy, EFP2 Coulomb, exchange-repulsion, polarization (induction), and dispersion energy terms were determined for dimers at the geometries used by Hohenstein and Sherrill and compared with the analogous terms obtained[9] using symmetry-adapted perturbation theory[28] (SAPT). Since the SAPT interaction energies obtained by Hohenstein and Sherrill are second-order or lower with respect to the intermolecular correlation operator, they are referred to as SAPT2 energies. The SAPT2 energies were computed with the aug-cc-pVDZ′ basis set, which consists of the cc-pVDZ basis set with the diffuse s and p functions of aug-cc-pVDZ added to non-hydrogen atoms.

Finally, a Monte Carlo/simulated annealing (MC/SA)[29] study was performed on the EFP2 benzene−pyridine and pyridine dimers to explore their respective potential energy surfaces. Temperature ranges of both 20 000−100 K and 3000−100 K were used. Geometry optimizations were performed every 10 steps during the MC/SA simulations.

RESULTS AND DISCUSSION

Sandwich. A comparison of EFP2 and CCSD(T) interaction energies and intermonomer separations at the respective potential energy minima of each sandwich dimer can be found in Table 1. The absolute differences between EFP2 and CCSD(T) energies for the minimum-energy sandwich dimer configurations range from 0.57 kcal/mol ($(Bz)_2$ S) to 0.90 kcal/mol ($(Py)_2$ S1). For the three pyridine-containing sandwich dimers, EFP2 predicts an optimum intermonomer separation 0.1 Å wider than that found with CCSD(T). The EFP2 optimum separation for $(Bz)_2$ S (3.9 Å) is identical to that found with CCSD(T).

Compared to the high-level CCSD(T) calculations,[9] the EFP2 potential energy curves (PECs) for the sandwich dimers are deeper (dimers are more strongly bound), by up to ∼0.9 kcal/mol. EFP2 and CCSD(T) predict a similar trend in the PEC ordering of the sandwich dimers (Figure 5). A slight difference occurs where the EFP2 PEC for $(Py)_2$ S1 drops below that of $(Bz)_2$ S; CCSD(T) calculations predict that the benzene sandwich dimer is always more strongly bound than $(Py)_2$ S1. The EFP2 potential energy minimum for $(Py)_2$ S1 is found to be −2.38 kcal/mol at a vertical separation of 3.9 Å, while that of the benzene sandwich dimer is −2.33 kcal/mol at 3.9 Å. With CCSD(T), $(Py)_2$ S1 has a potential minimum of −1.61 kcal/mol at 3.8 Å and $(Bz)_2$ S has a minimum of −1.76 kcal/mol at 3.9 Å.[9]

The root-mean-square deviation (RMSD) and maximum absolute (unsigned) difference in energy (MAX) between the EFP2 PEC and the corresponding CCSD(T) PEC for each sandwich structure are shown in Table 2. For each set of PECs, these values were computed on a subset of the PEC data beginning from the first negative (attractive) binding energy found with EFP2 and ending with the final computed binding energy at 7.0 Å. This subset was chosen to give the most meaningful comparison between EFP2 and CCSD(T), since the EFP2 PECs are significantly more repulsive than the CCSD(T) PECs at short intermonomer separations (closer than ∼3.6 Å for the sandwich dimers). The $(Bz)_2$ S PEC is in the closest agreement with CCSD(T), having the lowest RMSD (0.39 kcal/mol) and lowest

Table 2. Comparison of EFP2 and High-Level ab Initio Potential Energy Curves[a]

	rmsd	MAX
(Bz)2 S	0.39	0.59
Bz−Py S	0.53	0.84
(Py)2 S1	0.52	0.80
(Py)2 S2	0.66	1.08
(Bz)2 T	0.61	1.72
Bz−Py T1	0.64	1.97
Bz−Py T2	0.65	1.34
Bz−Py T3	0.31	0.47
Bz−Py T4	0.40	1.16
(Py)2 T1	0.34	1.03
(Py)2 T2	0.54	1.06
(Py)2 T3	0.64	1.94
(Py)2 T4	0.27	0.92
(Bz)2 P1a	0.70	1.31
(Bz)2 P1b	0.75	1.31
Bz−Py P1a	0.55	0.95
Bz−Py P1b	0.48	0.96
(Py)2 P1a	0.40	0.68
(Py)2 P1b	0.44	0.94
(Py)2 P2a	0.47	0.87
(Py)2 P2b	0.39	0.83
(Py)2 H-bonded*	0.33	0.50

[a] Root-mean-square deviation (rmsd) and maximum absolute (unsigned) energy difference (MAX) of EFP2 potential energy curves (PECs) compared to the high-level ab initio PECs of ref 9. For sandwich (S), T-shaped (T), and hydrogen-bonded dimers, the reference PECs were computed with CCSD(T) estimated to the complete basis set (CBS) limit, except where noted by (*). The (*) dimers are est. CCSD(T)/aug-cc-pVTZ. For parallel displaced dimers, the reference PECs were computed with SCS-MP2/aug-cc-pVTZ. Values are in kcal/mol.

dx.doi.org/10.1021/jp201039b |J. Phys. Chem. A 2011, 115, 4598–4609

Table 3. EFP2 and SAPT2 Contributions to the Interaction Energy of the Sandwich Configurations of Benzene, Benzene−Pyridine, and Pyridine Dimers[a]

	Coulomb	polarization	exch-rep	dispersion	total
$(Bz)_2$ S SAPT2	−0.48	−0.28	4.52	−5.68	−1.92
EFP2	−0.26	−0.36	4.38	−5.93	−2.17
Bz−Py S SAPT2	−0.80	−0.26	4.00	−5.34	−2.40
EFP2	−0.86	−0.27	3.66	−5.53	−3.00
$(Py)_2$ S1 SAPT2	−0.05	−0.21	3.57	−5.00	−1.69
EFP2	−0.25	−0.18	3.26	−5.19	−2.36
$(Py)_2$ S2 SAPT2	−1.29	−0.25	3.49	−5.00	−3.05
EFP2	−1.57	−0.20	3.08	−5.16	−3.85

[a] All sandwich dimers held at vertical separation R = 3.8 Å. Energies in kcal/mol. SAPT2 data, taken from ref 9 calculated with the aug-cc-pVDZ′ basis set.

MAX (0.59 kcal/mol). The greatest RMSD (0.66 kcal/mol) and MAX (1.08 kcal/mol) correspond to the $(Py)_2$ S2 PEC.

The EFP2 and SAPT2 contributions to the sandwich interaction energies at an intermonomer separation of 3.8 Å are summarized in Table 3. Since this is the distance at which the SAPT analyses are available,[9] it was chosen for consistency. Consequently, the EFP2 total interaction energies that are listed in Tables 1 and 3 are different. Those in Table 1 are more quantitatively meaningful, since they correspond to potential energy minima on the respective potential energy surfaces. The predominant attractive term in sandwich dimer interactions is the dispersion energy, due to direct overlap of the π electron clouds. However, this overlap also produces a large exchange-repulsion energy. Compared to benzene, pyridine has a more contracted, less polarizable π cloud. This causes dispersion interactions among pyridine-containing sandwich dimers to be slightly less favorable to binding, but it also decreases the magnitude of the exchange-repulsion term. As shown in Table 3, the $(Py)_2$ sandwich configurations have dispersion energies that are approximately 0.3 kcal/mol higher (less stabilized) than those of the Bz−Py sandwich dimer, which in turn has a dispersion energy that is approximately 0.3 kcal/mol (with SAPT2) or 0.4 kcal/mol (with EFP2) higher than the $(Bz)_2$ sandwich dimer. However, the exchange-repulsion energy is reduced accordingly. Overall, this decrease in the exchange-repulsion interaction energy makes pyridine-containing sandwich dimers more likely to be more strongly bound than the benzene sandwich dimer, despite the concomitant decrease in favorable dispersion interactions.

The exception to the above analysis is $(Py)_2$ S1, which is the least strongly bound sandwich dimer except at short intermonomer distances ($R \leq 3.6$ Å with estimated CCSD(T)/CBS; $R \leq 3.9$ Å with EFP2), where it becomes slightly more strongly bound than the benzene sandwich dimer. Even though the dispersion and exchange-repulsion terms associated with $(Py)_2$ S1 follow the trends described above, the Coulomb term is only marginally favorable to binding, due to parallel dipole−dipole interactions. The Coulomb term in $(Py)_2$ S1 contributes only −0.05 kcal/mol (SAPT2) or −0.25 kcal/mol (EFP2) to the total interaction energy at an intermonomer separation R = 3.8 Å. This is less than or equal to the Coulomb term in the benzene dimer, which is −0.48 kcal/mol (SAPT2) or −0.26 kcal/mol (EFP2) at R = 3.8 Å. In contrast, $(Py)_2$ S2, which has antiparallel dipole−dipole interactions, exhibits a significantly stronger Coulomb interaction of −1.29 kcal/mol (SAPT2) or −1.57 kcal/mol (EFP2) at the same separation. The Coulomb term in Bz−Py S falls in between that of $(Bz)_2$ S and $(Py)_2$ S1 at both the SAPT2 and EFP2 levels of theory (Table 3).

Table 4. EFP2 and SAPT2 Contributions to the Interaction Energy of the T-Shaped Configurations of Benzene, Benzene−Pyridine, and Pyridine Dimers[a]

	R	Coulomb	polarization	exch-rep	dispersion	total
$(Bz)_2$ T SAPT2	5.0	−1.75	−0.52	3.52	−3.73	−2.48
EFP2		−2.94	−0.35	5.04	−4.59	−2.84
Bz−Py T1 SAPT2	5.0	−2.12	−0.64	3.54	−3.70	−2.92
EFP2		−3.32	−0.45	4.94	−4.34	−3.17
Bz−Py T2 SAPT2	4.7	0.33	−0.62	3.38	−3.75	−0.66
EFP2		1.97	−0.59	3.10	−4.35	0.13
Bz−Py T3 SAPT2	5.0	−1.21	−0.40	3.27	−3.51	−1.85
EFP2		−1.77	−0.15	3.07	−3.68	−2.53
Bz−Py T4 SAPT2	5.0	−1.80	−0.49	3.21	−3.36	−2.44
EFP2		−2.06	−0.29	2.91	−3.36	−2.80
$(Py)_2$ T1 SAPT2	5.0	−1.39	−0.50	3.29	−3.48	−2.08
EFP2		−2.00	−0.23	3.04	−3.50	−2.69
$(Py)_2$ T2 SAPT2	4.7	−0.39	−0.54	3.17	−3.53	−1.29
EFP2		1.14	−0.56	3.74	−4.70	−0.38
$(Py)_2$ T3 SAPT2	5.0	−1.78	−0.38	2.67	−3.11	−2.60
EFP2		−2.11	−0.23	3.12	−3.61	−2.83
$(Py)_2$ T4 SAPT2	5.0	−1.14	−0.38	2.78	−3.12	−1.86
EFP2		−1.10	−0.19	2.34	−3.15	−2.10

[a] Monomer center to monomer center distance R given in Å. Energies given in kcal/mol. SAPT2 data, taken from ref 9, calculated with the aug-cc-pVDZ′ basis set.

T-Shaped. The interaction energies for the T-shaped dimers are also listed in Table 1. The absolute differences between EFP2 and CCSD(T) energies (Table 1) for the T-shaped dimers range from 0.01 kcal/mol ($(Py)_2$ T4) to 0.78 kcal/mol ($(Py)_2$ T2). As with the sandwich structures, EFP2 tends to favor a slightly larger (0.1−0.2 Å) intermonomer separation for the T-shaped dimers compared to CCSD(T). For one dimer (Bz−Py T1), EFP2 finds an optimum separation 0.3 Å wider than CCSD(T); for two dimers (Bz−Py T3 and $(Py)_2$ T1), EFP2 and CCSD(T) optimum intermonomer separations agree exactly.

As described in ref 9, binding in the T-shaped dimers is stabilized by the Coulomb energy due to the role of pyridine as a "π-hydrogen bond" donor. By pulling electron density away from the hydrogen atom that is para to the heteroatom, the heteroatom in pyridine gives this para hydrogen a greater positive charge compared to its value in benzene. The Coulomb contribution to the binding energy in the pyridine-containing T-shaped dimers comes largely from the interaction of the positive para hydrogen atom on one monomer with the negative π cloud of the other monomer ring. The same change in electron density that makes the pyridine para hydrogen more positive also makes the pyridine π cloud less diffuse, decreasing its ability to act as a "π-hydrogen bond" acceptor. This is reflected in the lower (in magnitude) binding energies of $(Py)_2$ T1 and T4 complexes relative to the corresponding Bz−Py T-shaped complexes.

The contributions to the T-shaped interaction energies follow a similar pattern to those for the sandwich isomers, as illustrated in Table 4. Note that, as discussed above with regard to Table 3, the distances used for the analysis in Table 4 are different from those in Table 1, and therefore, the total interaction energies

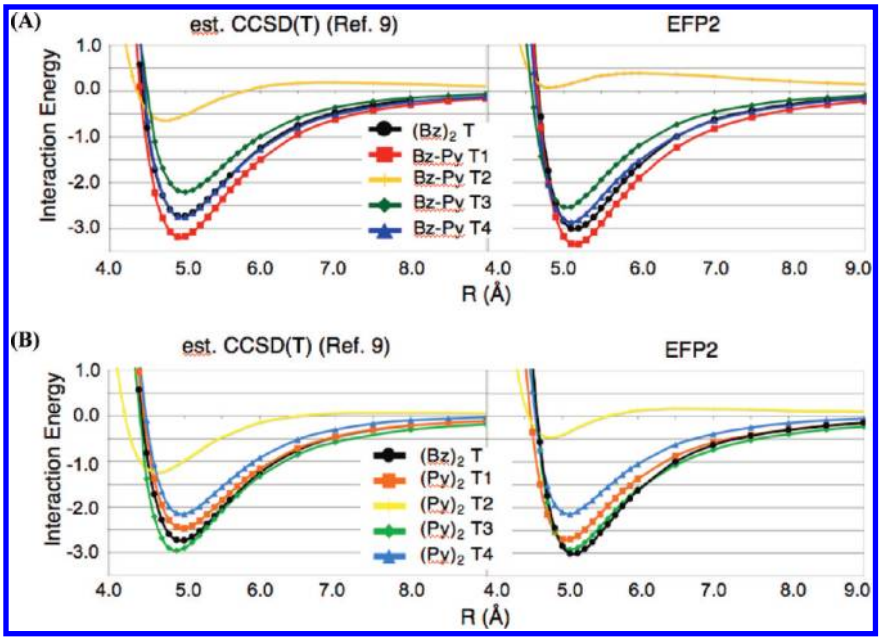

Figure 6. Est. CCSD(T)/CBS[9] (left) and EFP2 (right) potential energy curves for the benzene−pyridine (A) and pyridine (B) T-shaped dimers. Interaction energy is in kcal/mol.

differ as well. While the dispersion energy is the largest attractive energy term for the T-shaped dimers (Table 4), the exchange-repulsion energy generally has a similar magnitude. The Coulomb term consequently makes significant contributions to the overall binding energy. When the Coulomb term is least attractive or is even repulsive (T2 complexes, in which the partially negative heteroatom interacts most directly with the π cloud of the other monomer ring), the complex may be very weakly bound, or not bound at all. EFP2 predicts a more repulsive Coulomb interaction in the T2 complexes compared to SAPT2, and therefore a more weakly bound dimer. Because the EFP2 Bz−Py T2 Coulomb interaction is more than 1 kcal/mol larger than that predicted by SAPT2,[9] EFP predicts this species to be unbound, whereas it is slightly (0.66 kcal/mol) bound according to SAPT2. EFP2 predicts $(Py)_2$ T2 to be more weakly bound than does SAPT2 for similar reasons. As shown in Table 1, the estimated CCSD(T) interaction energies are similar to those predicted by SAPT2. For the other T complexes, EFP2 and SAPT2 are in good agreement, within ∼0.2−0.6 kcal/mol (Table 4), with the EFP2 dimers more strongly bound. Each of the contributing interactions is also in good agreement. In these dimers, EFP2 tends to overestimate the Coulomb attraction to some degree compared to SAPT2 and to slightly (∼0.2 kcal/mol) underestimate the magnitude of the polarization.

A comparison of the CCSD(T)[9] and EFP2 PECs for the T-shaped dimers is shown in Figure 6. The EFP2 curves tend to be somewhat deeper (more strongly bound) and slightly right-shifted (larger intermonomer separation) compared to the CCSD(T) curves. This is consistent with the results of previous EFP2 studies on benzene[5] and substituted benzene[7] dimers. The ordering of the EFP2 and CCSD(T) curves is very similar, although EFP2 overbinds the T-shaped benzene dimer somewhat more than it does the other T-shaped dimers, resulting in some minor differences. The CCSD(T) Bz−Py T4 curve, for example, nearly coincides with the CCSD(T) $(Bz)_2$ T curve, while the EFP2 $(Bz)_2$ T curve is slightly deeper than that of Bz−Py T4. Similarly, whereas CCSD(T) shows the $(Bz)_2$ T curve always above $(Py)_2$ T4, the two nearly coincide when EFP2 is used.

RMSD values and maximum energy differences (MAX) between EFP2 and CCSD(T) T-shaped dimer PECs appear in Table 2. As with the sandwich dimers, these statistics were calculated on a subset of data beginning from the first negative (attractive) EFP2 binding energy for each dimer and ending with the final computed binding energy (at 8.0 Å for T-shaped dimers). In the case of Bz−Py T2, for which EFP2 finds no net binding, statistics were calculated beginning with the first attractive CCSD(T) binding energy. $(Py)_2$ T4 shows the best agreement between EFP2 and CCSD(T) curves, with a RMSD of 0.27 kcal/mol and a MAX of 0.92 kcal/mol. $(Bz)_2$ T, Bz−Py T1, Bz−Py T2, and $(Py)_2$ T3 show the greatest discrepancy between their EFP2 and CCSD(T) PECs, with RMSD values in the range of 0.61−0.65 kcal/mol. The greatest maximum difference between EFP2 and CCSD(T) energies (1.97 kcal/mol) is found in the Bz−Py T1 dimer. However, much of the difference between EFP2 and CCSD(T) energies results from EFP2 underbinding at short (equilibrium distance minus 0.4 Å, or less) intermonomer separations. If RMSD values and maximum energy differences are calculated beginning from 0.3 Å closer than the EFP2 equilibrium distance, for example, the Bz−Py T1 dimer's RMSD decreases from 0.64 to 0.39 kcal/mol and the MAX decreases from 1.97 to 0.53 kcal/mol.

Parallel Displaced. Potential energy curves for the parallel displaced dimers are shown in Figure 7, where EFP2 interaction energies are compared with SCS-MP2/aug-cc-pVTZ interaction energies from ref 9. These curves correspond to parallel displaced dimers with a vertical displacement held fixed at R = 3.5 Å while the horizontal displacement, H, was varied in increments of 0.2 Å. Interaction energies and horizontal displacements of the most favorable of these structures appear in Table 5. The absolute energy differences between EFP2 and SCS-MP2 for these parallel displaced structures (Table 5) range from

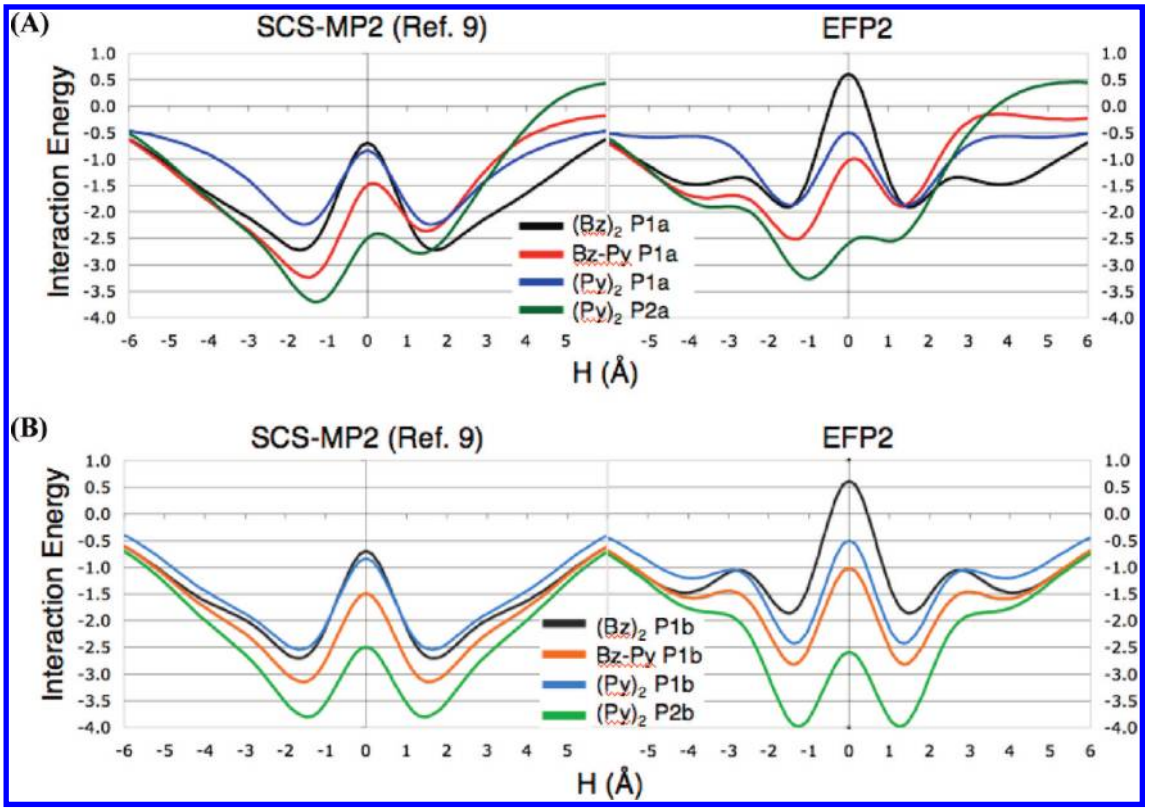

Figure 7. SCS-MP2/aug-cc-pVTZ[9] (left) and EFP2 (right) potential energy curves for the parallel displaced dimers with a vertical separation $R = 3.5$ Å. (A) "Over vertex" displaced dimers, in which the displacement is over the heteroatom. (B) "Edgewise" displaced dimers, in which the displacement is over the C−C bond of carbons 2 and 3. Interaction energy is in kcal/mol.

Table 5. EFP2 and SCS-MP2 Interaction Energies of Parallel Displaced Configurations of Benzene, Benzene−Pyridine, and Pyridine Dimers[a]

	H	SCS-MP2	EFP2
$(Bz)_2$ P1a	1.6	−2.71	−1.90
$(Bz)_2$ P1b	1.6	−2.70	−1.84
Bz−Py P1a(+)	1.4	−2.36	−1.88
Bz−Py P1a(−)	1.6	−3.23	−2.43
Bz−Py P1b	1.6	−3.14	−2.71
$(Py)_2$ P1a	1.6	−2.24	−1.85
$(Py)_2$ P1b	1.6	−2.54	−2.31
$(Py)_2$ P2a(+)	1.4	−2.78	−2.44
$(Py)_2$ P2a(−)	1.2	−3.70	−3.21
$(Py)_2$ P2b	1.4	−3.80	−3.94

[a] Vertical displacement $R = 3.5$ Å. Horizontal displacement H is given in Å. Energies are given in kcal/mol. SCS-MP2/aug-cc-pVTZ data is from ref 9.

0.14 kcal/mol ($(Py)_2$ P2b) to 0.86 kcal/mol ($(Bz)_2$ P1b), with an average difference of 0.50 kcal/mol.

RMSD values and maximum absolute energy differences between EFP2 and SCS-MP2 PECs for the parallel displaced dimers can be found in Table 2. Of the EFP2 parallel displaced PECs, those for the benzene dimers ($(Bz)_2$ P1a and $(Bz)_2$ P1b) differ the most from the corresponding SCS-MP2 PECs, having RMSD values of 0.70 and 0.75 kcal/mol, respectively. The maximum absolute energy difference is 1.31 kcal/mol for both $(Bz)_2$ PECs. RMSD values for the pyridine-containing parallel displaced dimers are lower, ranging from 0.39 kcal/mol ($(Py)_2$ P2b) to 0.55 kcal/mol (Bz−Py P1a). The maximum energy differences for pyridine-containing dimers are all under 1 kcal/mol, with $(Py)_2$ P1a having the lowest maximum difference at 0.68 kcal/mol.

Changes in the curvature of EFP2 potential energy curves for the parallel displaced structures (Figure 7) can be seen at horizontal separations in the range of 2−4 Å (and −2 to −4 Å). In some cases, these curvature changes give rise to small dips in the potential energy surface that do not correspond to features on the SCS-MP2 potential energy curves (Figure 7). However, the dips are well above the minimum energies found along these curves, and the overall correspondence between the EFP2 and SCS-MP2 curves is strong (Table 2).

The most favorable structure, predicted by both EFP2 and SCS-MP2,[9] is $(Py)_2$ P2b, due to its antiparallel dipoles. For all other parallel displaced structures around their energy minima, EFP2 predicts a somewhat smaller binding energy than does SCS-MP2, but EFP2 slightly overbinds the $(Py)_2$ P2b structure by ∼0.14 kcal/mol. The next most favorable parallel displaced configuration, $(Py)_2$ P2a(−), is about 0.2 (0.7) kcal/mol higher in energy according to SCS-MP2 (EFP2). The Bz−Py P1a(−) and Bz−Py P1b complexes are next lowest in energy. Both SCS-MP2 and EFP2 predict these two dimers to be very close to each other in energy. While SCS-MP2 predicts that $(Py)_2$ P1a and $(Py)_2$ P1b have a smaller binding energy than $(Bz)_2$ P1a and $(Bz)_2$ P1b, respectively (due to parallel dipoles), EFP2 underbinds the $(Bz)_2$ dimers and reverses this energy ordering.

Table 6. EFP2 and SAPT2 Contributions to the Interaction Energy of the Parallel Displaced Configurations of Benzene, Benzene−Pyridine, and Pyridine Dimers[a]

	Coulomb	polarization	exch-rep	dispersion	total
(Bz)2 P1a SAPT2	−2.77	−0.88	8.58	−7.88	−2.95
EFP2	−2.09	−0.47	9.70	−8.12	−0.98
(Bz)2 P1b SAPT2	−2.81	−0.91	8.68	−7.88	−2.92
EFP2	−2.10	−0.47	9.79	−8.12	−0.90
Bz−Py P1a(+) SAPT2	−1.91	−0.73	7.24	−7.16	−2.55
EFP2	−1.01	−0.36	7.60	−7.39	−1.16
Bz−Py P1a(−) SAPT2	−3.24	−0.85	8.25	−7.59	−3.43
EFP2	−2.60	−0.38	9.21	−7.79	−1.56
Bz−Py P1b SAPT2	−2.95	−0.81	7.77	−7.38	−3.37
EFP2	−2.49	−0.36	8.45	−7.62	−2.02
(Py)2 P1a SAPT2	−1.74	−0.68	6.97	−6.90	−2.35
EFP2	−1.05	−0.27	7.15	−7.07	−1.24
(Py)2 P1b SAPT2	−2.04	−0.66	7.01	−6.93	−2.62
EFP2	−1.63	−0.25	7.32	−7.16	−1.71
(Py)2 P2a(+) SAPT2	−1.78	−0.66	5.90	−6.46	−2.99
EFP2	−0.56	−0.33	5.64	−6.68	−1.93
(Py)2 P2a(−) SAPT2	−3.54	−0.79	7.93	−7.30	−3.70
EFP2	−3.01	−0.28	8.80	−7.48	−1.98
(Py)2 P2b SAPT2	−3.26	−0.70	6.85	−6.89	−4.00
EFP2	−2.98	−0.26	7.08	−7.13	−3.30

[a] Vertical displacement R = 3.4 Å; horizontal displacement H = 1.6 Å. Energies are given in kcal/mol. SAPT2 data is from ref 9.

EFP2 tends to favor a slightly larger (0.05−0.25 Å) intermonomer separation in sandwich-type structures: it underestimates the Coulomb attraction and overestimates the exchange-repulsion at shorter distances.[5,7] (See also the optimal intermonomer distances listed in Table 1.) It was demonstrated previously[5] that EFP2 will produce parallel displaced benzene dimer interaction energies that are closer to the CCSD(T) values when the EFP2 structures are allowed to relax to their slightly more separated equilibrium values. For example, a previous comparison[5] with CCSD(T) potential energy curves for the parallel displaced benzene dimer[30] shows that the $(Bz)_2$ equilibrium geometry is R = 3.6 Å, H = 1.6 Å with CCSD(T) but R = 3.8 Å, H = 1.2 Å with EFP2. As a result, the EFP2 curve at R = 3.4 Å lies 2.5−4.0 kcal/mol higher in energy than the CCSD(T) curve. However, the EFP2 curve at R = 3.8 Å follows the corresponding CCSD(T) curve very closely.[5] The same may be true for heteroatom-containing dimers as well.

EFP2 and SAPT2 energy decompositions for the parallel displaced configurations with vertical displacement R = 3.4 Å and horizontal displacement H = 1.6 Å are given in Table 6. In light of the above discussion, this intermonomer separation may be well below the optimal separation found with EFP2; consequently, the agreement here with SAPT2 is not as favorable, but this is the only intermonomer separation for which the SAPT analysis is available. Compared to SAPT2, EFP2 tends to underestimate the Coulomb attraction in these dimers by about 0.5 kcal/mol. The closest agreement is in $(Py)_2$ P2b, where the EFP2 underestimation is 0.28 kcal/mol, and the greatest difference is in $(Py)_2$ P2a(+), with an EFP2 underestimation of 1.22 kcal/mol. The EFP2 polarization attraction is about half that of the SAPT2 polarization. EFP2 overestimates the exchange-repulsion of the $(Bz)_2$ dimers by more than 1 kcal/mol. These

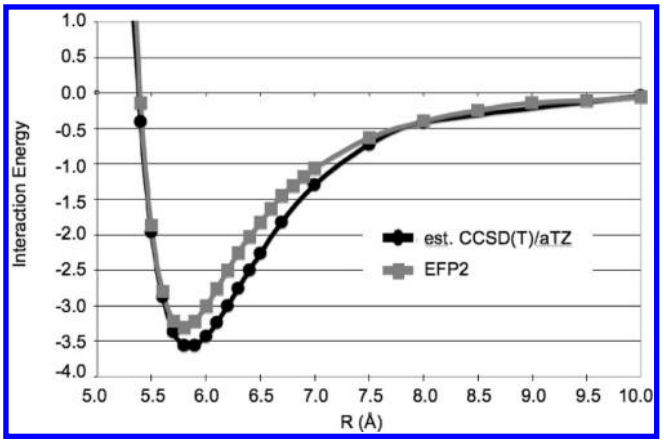

Figure 8. Est. CCSD(T)/aug-cc-pVTZ[9] and EFP2 potential energy curves for the hydrogen-bonded pyridine dimer. Interaction energy is in kcal/mol.

dimers are the least strongly bound and have an EFP2 total interaction energy differing from the SAPT2 total interaction energy by about 2 kcal/mol (less strongly bound with EFP2). The EFP2 and SAPT2 comparisons for Bz−Py P1a(−) and $(Py)_2$ P2a(−) are similar, with an exchange-repulsion 0.96 and 0.87 kcal/mol (respectively) higher with EFP2 and a total interaction energy 1.87 and 1.72 kcal/mol (respectively) less strongly bound with EFP2. Otherwise, the EFP2 total interaction energies differ from those of SAPT2 by less than 1.4 kcal/mol. EFP2 dispersion energies are in excellent agreement with SAPT2, being consistently about 0.2 kcal/mol more attractive.

Hydrogen Bonded. EFP2 agrees well with the estimated CCSD(T)/aug-cc-pVTZ results of ref 9 for the hydrogen-bonded dimer. The H-bonded dimer is illustrated in Figure 4, and the potential energy curves are shown in Figure 8. For potential energies between 5.4 and 10 Å, the maximum energy difference between the EFP2 and CCSD(T) values is 0.50 kcal/mol (Table 2). The root-mean-square deviation between the two PECs is 0.33 kcal/mol (Table 2). Est. CCSD(T)/aug-cc-pVTZ finds the potential minimum for the hydrogen-bonded dimer to be −3.56 kcal/mol at an intermonomer separation (ring center to ring center distance) of 5.8 Å, corresponding to hydrogen bond distances of 2.5 Å. EFP2 finds the minimum to be −3.3 kcal/mol at the same intermonomer separation. At this energy minimum, the Coulomb term is −3.62 kcal/mol, the exchange repulsion is 3.95 kcal/mol, the polarization is −0.64 kcal/mol, and the dispersion is −2.99 kcal/mol with EFP2. The magnitude of the exchange-repulsion exceeds that of the Coulomb term by 0.3 kcal/mol. Thus, although the hydrogen-bonded configuration exhibits the smallest dispersion interaction in terms of magnitude (compared to the dispersion interaction of the sandwich and T-shaped complexes given in Tables 3-4), the dispersion energy is necessary for the overall binding of this complex.

Monte Carlo/Simulated Annealing (MC/SA). The primary focus of this investigation has been on the pyridine and benzene−pyridine structures that have been most commonly studied by high-level electronic structure methods. However, the accuracy and computational efficiency of the EFP method suggests that an extensive search for other minima should be carried out. Consequently, a series of Monte Carlo/simulated annealing (MC/SA) searches were performed.

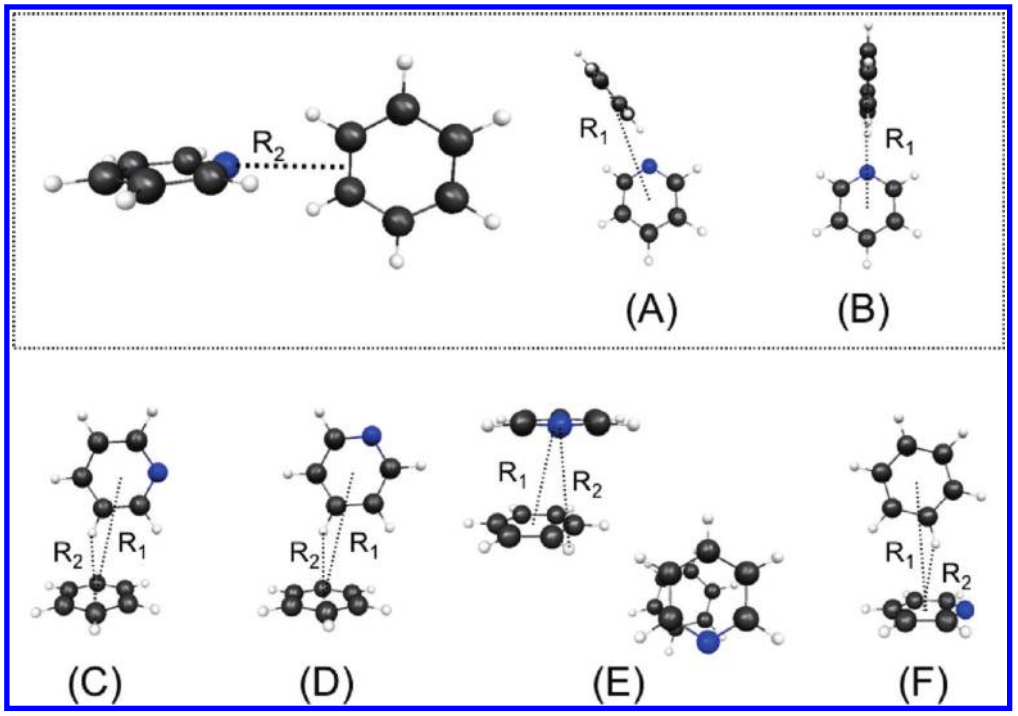

Figure 9. Selected structures found with EFP2 Monte Carlo/simulated annealing (MC/SA) for the benzene−pyridine dimer, in order of strongest to weakest interaction energy. (A) is the lowest energy structure observed. (B) is a transition state between two symmetry-equivalent structures like (A). (C), (D), and (F) are T-like structures, while (E) is a twisted parallel-displaced-type structure. Two views of (E) are shown to illustrate the relative orientation of the monomers. R_1 indicates the distance between monomer centers. For (A) and (B), R_2 indicates the distance between the pyridine heteroatom and the midpoint of the nearest benzene carbon−carbon bond. For (C), (D), and (F), R_2 is the distance from a ring center of one monomer to the nearest hydrogen atom on the other monomer. For (E), R_2 is the distance from the pyridine heteroatom to the nearest benzene hydrogen. Distances and interaction energies of all complexes appear in Table 7, while interaction energy components of global minimum structure (A) appear in Table 8.

Important structural motifs found with the EFP2 MC/SA simulations for the benzene−pyridine and pyridine dimers are shown in Figures 9 and 10, respectively. Except where noted otherwise, all structures have positive definite Hessians (matrices of second derivatives of the energy with respect to the geometry), indicating that they are minima on the potential energy surface. Very tight gradient convergent criteria were employed for the geometry optimizations. Interaction energies for these structures and the intermonomer distances R_1 and R_2 indicated in Figures 9 and 10 appear in Table 7. R_1 is the distance between ring centers for all geometries shown. For the lowest energy structures (9A, 10A), R_2 is the distance between the pyridine heteroatom and the nearest carbon−carbon bond midpoint on the other monomer. The definition of R_2 for other geometries is given in Figures 9 and 10.

The lowest energy geometries for Bz−Py and $(Py)_2$ are very similar (Figures 9A and 10A). Both structures are found to involve the negatively charged pyridine heteroatom interacting with the positive hydrocarbon backbone of the second monomer. The distance from the pyridine nitrogen to the nearest C−C bond midpoint on the other monomer (R_2) is 3.09 Å for Bz−Py and 3.06 Å for $(Py)_2$. In the Bz−Py lowest energy structure, a line bisecting the pyridine ring through the heteroatom would form a 155° angle with the line given by R. The $(Py)_2$ lowest energy structure has a similar configuration, in which this angle is 156°. A Bz−Py structure in which this angle is 180° (Figure 9B) was found with EFP2 MC/SA (R = 3.10 Å). This structure, which is 0.43 kcal/mol higher in energy than the minimum energy structure, has one imaginary frequency (23.83 cm^{-1}), indicating that the structure in Figure 9B is a transition state between two symmetry-equivalent minima of the Bz−Py dimer. No structure similar to Figure 9B was found by the MC/SA simulations for the $(Py)_2$ dimer.

The EFP2 interaction energy components for the lowest energy geometries found with the MC/SA simulations (Figure 9A, 10A) are given in Table 8. Both structures have exchange-repulsion terms of approximately 6.5 kcal/mol and have correspondingly large Coulomb interaction terms as well: −6.10 kcal/mol for Bz−Py MC/SA, −6.85 kcal/mol for $(Py)_2$ MC/SA (Table 7). Due to the angle between the monomers (described above), which brings the ortho hydrogen of pyridine closer to the π cloud of the other monomer, the dispersion interaction energy is also large for these structures. This creates a "π-hydrogen bond" effect similar to that which occurs in the T-shaped dimers. The dispersion energy of the Bz−Py global minimum structure 9A (−4.33 kcal/mol, Table 7) is approximately the same as that of Bz−Py T1 (−4.34 kcal/mol) or Bz−Py T2 (−4.35 kcal/mol, Table 4). The dispersion energy of the $(Py)_2$ global minimum structure is a very similar −4.34 kcal/mol (Table 7), greater than that of any $(Py)_2$ T-shaped structures except $(Py)_2$ T2 (−4.70 kcal/mol, Table 4). Thus, while the Coulomb term is the single largest attractive energy term for Bz−Py 9A, the structure would not be bound without the dispersion interaction. The $(Py)_2$ lowest energy structure 10A is very similar to that found for Bz−Py. Overall, $(Py)_2$ 10A is 0.71 kcal/mol more strongly bound than Bz−Py 9A, due mainly to a larger Coulomb attraction.

dx.doi.org/10.1021/jp201039b |J. Phys. Chem. A 2011, 115, 4598–4609

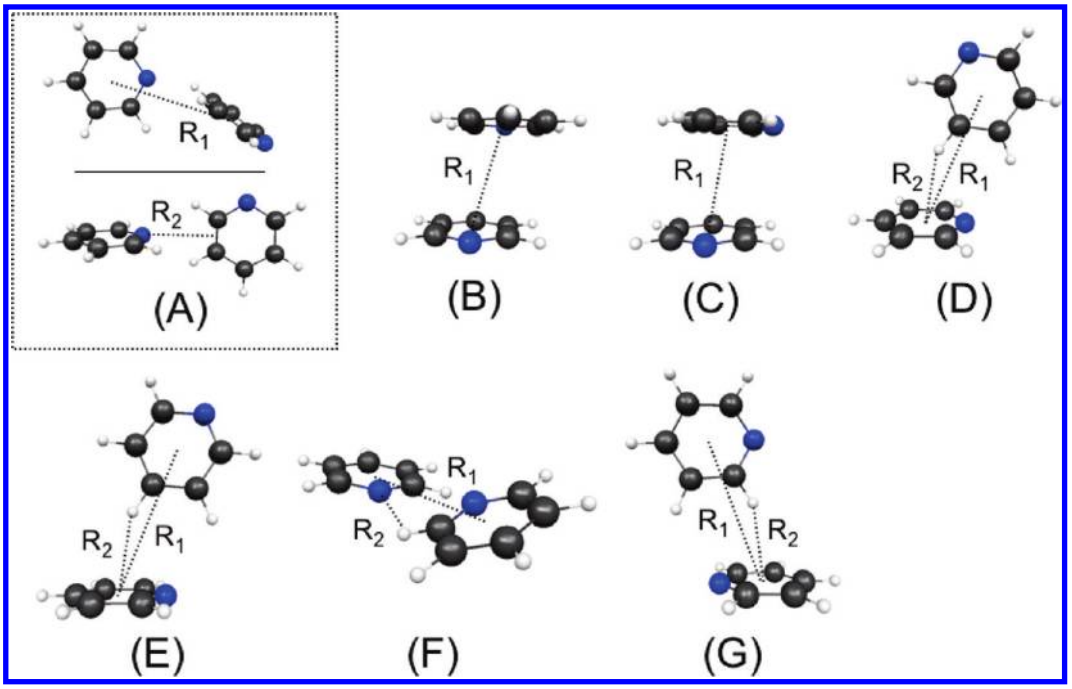

Figure 10. Selected structures found with EFP2 Monte Carlo/simulated annealing (MC/SA) for the pyridine dimer, in order of strongest to weakest interaction energy. (A) is the lowest energy structure observed. (B) and (C) are parallel displaced type structures. (D), (E), and (G) are T-like structures. (F) is a nonplanar hydrogen-bonded structure. R_1 indicates the distance between monomer centers. For (A), R_2 indicates the distance between the pyridine heteroatom and the midpoint of the nearest benzene carbon−carbon bond. For (D), (E), and (G), R_2 is the distance from a ring center of one monomer to the nearest hydrogen atom on the other monomer. For (F), R_2 indicates the length of the hydrogen bond. For (B) and (C), an R_2 value is not defined. Distances and interaction energies of all complexes appear in Table 7, while interaction energy components of global minimum structure (A) appear in Table 8.

Table 7. EFP2 Interaction Energies and Intermonomer Distances of Selected Bz−Py and $(Py)_2$ Structures Found with EFP2 Monte Carlo/Simulated Annealing (MC/SA)[a]

	R_1	R_2	ΔE
	Bz−Py		
A	5.55	3.09	−4.68
B	5.71	3.10	−4.25
C	4.96	2.64	−3.63
D	4.98	2.65	−3.60
E	3.87	3.64	−3.46
F	4.94	2.56	−3.19
	(Py)2		
A	5.53	3.06	−5.39
B	3.80		−4.23
C	3.79		−4.11
D	4.93	2.61	−4.10
E	4.96	2.63	−3.83
F	5.55	2.44	−3.70
G	4.92	2.65	−3.67

[a] Interaction energies ΔE (kcal/mol) and intermonomer distances R_1 and R_2 (Å) of the structures shown in Figures 9 and 10. R_1 is the distance between monomer centers in all cases. R_2 is defined in Figures 9 and 10 for each structure.

While the $(Py)_2$ 10A structure would still be weakly bound without the dispersion interaction, the dispersion interaction does contribute −4.34 kcal/mol to the binding energy.

Table 8. EFP2 Energy Contributions to the Global Minimum Benzene−Pyridine and Pyridine Dimer Structures Found with EFP2 Monte Carlo/Simulated Annealing[a]

	Coulomb	polarization	exch-rep	dispersion	total
Bz−Py MC/SA	−6.10	−0.68	6.43	−4.33	−4.68
(Py)2 MC/SA	−6.85	−0.79	6.59	−4.34	−5.39

[a] Energies in kcal/mol.

For the Bz−Py dimer, in addition to the lowest energy structure 9A and the transition state 9B, structures resembling T-shaped (Figure 9C, D, F) and parallel displaced (Figure 9E) motifs were also found. The T-like structure 9C resembles Bz−Py T4, although the ring center of pyridine does not lie directly over the ring center of benzene as in the artificially constrained Bz−Py T4. In structure 9C, the meta carbon of pyridine is closest to the benzene ring center. The T-like structure 9D is similar to 9C, but the para carbon of pyridine lies most directly over the benzene ring center. Structures 9C and 9D are nearly degenerate in energy, differing by only 0.03 kcal/mol. They are, respectively, 1.05 and 1.08 kcal/mol higher in energy than the lowest energy structure 9A (Table 7). The parallel displaced structure 9E most closely resembles Bz−Py P1b, although the monomers in 9E are rotated compared to their orientation in Bz−Py P1b. This dimer configuration is 1.22 kcal/mol less strongly bound than the lowest energy configuration 9A (Table 7). Finally, the T-like structure 9F is most similar to Bz−Py T3, in that a benzene hydrogen atom lies over the pyridine ring. However, compared to its orientation in Bz−Py T3, the benzene in 9F is rotated 90° relative to pyridine. Also, as

with the other T-like structures, the ring centers do not lie directly over one another. This structure is 1.49 kcal/mol higher in energy than the minimum energy structure 9A (Table 7).

Due to the lower symmetry of pyridine compared to benzene, the potential energy surface of $(Py)_2$ is even more diverse than that of Bz−Py. A selection of unique structures found with MC/SA are shown in Figure 10, with structure 10A being the lowest in energy. Structures 10B and 10C are parallel displaced structures with different orientations of the pyridine monomers. The more energetically favorable (10B) has antiparallel pyridines, similar to $(Py)_2$ P2b, while in the other (10C), the pyridine heteroatoms are offset by 90°. These structures differ in energy by 0.12 kcal/mol, with the antiparallel structure (10B) 1.16 kcal/mol higher in energy than the minimum energy configuration 10A (Table 7). Structures 10D, 10E, and 10G are T-shaped type, although the monomers are offset: the center of the "top" monomer does not lie directly above the ring plane of the other. Structure 10G most closely resembles $(Py)_2$ T3, with the "top" monomer displaced over the heteroatom of the other. The geometries of 10D and 10E do not directly correspond to any of the constrained T-shaped structures examined previously in this study; in addition to the offset monomer centers, the "top" pyridine is rotated ∼60° compared to its orientation in otherwise similar constrained structures (e.g., $(Py)_2$ T3). The T-shaped structure 10D, at −4.10 kcal/mol, is nearly isoenergetic with the parallel displaced structure 10C, at −4.11 kcal/mol (Table 7). Configurations 10D, 10E, and 10G are respectively 1.29, 1.56, and 1.72 kcal/mol higher in energy than the minimum energy configuration 10A (Table 7). Figure 10F has a nonplanar hydrogen-bonded structure. A planar H-bonded geometry was not found with the MC/SA simulations, and an EFP2 geometry optimization beginning from the geometry of the most energetically favorable planar H-bonded structure examined previously in this study yields a second-order saddle point. The nonplanar H-bonded structure (10F) lies 1.69 kcal/mol above the minimum energy geometry (Table 7).

The offset T-shaped (Figure 9C, 9D, 9F, 10D, 10E, 10G) and parallel displaced (9E, 10B, 10C) structures found with the EFP2 MC/SA simulations have analogues on the benzene dimer potential energy surface. A previous EFP2 MC/SA study[7] that included the benzene dimer found structures similar to those discussed above. For the benzene dimer, the EFP2 lowest energy structure is offset T-shaped, with a monomer center-to-center distance (R_1) of 5.1 Å and an interaction energy of −2.80 kcal/mol. A parallel displaced structure with R_1 = 4.0 Å has an interaction energy of −2.41 kcal/mol. Finally, an edge-to-edge configuration of the benzene dimer similar to 9B, with R_1 = 6.2 Å, has an interaction energy of −1.53 kcal/mol. These EFP2 results are similar to the findings of a previous study[23] examining 491 configurations of the benzene dimer. Energies computed with MP2/aug-cc-pVTZ + ΔCCSD(T) correction of similar offset T-shaped, parallel displaced, and edge-to-edge structures are reported as −2.795, −2.699, and −1.805 kcal/mol, respectively; these structures are also reported to be true minima, rather than saddle points.

The EFP2 MC/SA results can also be compared with results from a DFT-D study[10] of the pyridine dimer potential energy surface. A structure similar to 10E and a planar hydrogen-bonded structure were found with DFT-D.[10] The DFT-D structure had a hydrogen to ring center distance R_2 of 2.66 Å (ref 10) compared to 2.63 Å found by EFP2 (Table 7). The EFP2 interaction energy for this structure is −3.8 kcal/mol (Table 7), compared to −3.1 kcal/mol with SCS-MP2, −4.2 kcal/mol with MP2, and −3.0 kcal/mol with DFT-D. As noted above, EFP2 finds a planar H-bonded structure (with hydrogen bond lengths R_2 = 2.44 Å vs 2.54 Å with the DFT-D[10] optimization) that is a second-order saddle point. The authors of the DFT-D study performed a full geometry optimization and noted that use of constrained monomer geometries altered the results of the study.[10] It is possible that the lack of planarity of the optimum EFP2 H-bonded structure results from the use of rigid monomers; however, no mention is made of Hessian calculations in ref 10 so it is not known whether the H-bonded structure reported there is a true minimum. An edge-to-edge structure like the EFP2 global minimum 10A is not reported in the DFT-D study.[10]

Cartesian coordinates and interaction energy components for the MC/SA structures described above are available online as Supporting Information.

CONCLUSIONS

For dimers of benzene, pyridine, and benzene−pyridine, the general effective fragment potential method (EFP2) is in good agreement with the high-level CCSD(T), MP2, and SAPT2 results of Hohenstein and Sherrill.[9] Consistent with previous studies on benzene dimers[5] and substituted benzene dimers,[7] EFP2 is found to slightly overestimate binding energies and intermonomer separations in sandwich structures and T-shaped structures other than those of type T2. EFP2 underestimates the Coulomb attraction in Bz−Py T2 and $(Py)_2$ T2, resulting in no bound state for the former and a weakly bound minimum for the latter. Slight differences in the energy order of the T-shaped dimer curves arise because EFP2 overbinds the T-shaped benzene dimer slightly more than other T-shaped structures. However, EFP2 underbinds parallel displaced benzene dimers more than it underbinds other parallel displaced structures.

Overall, the differences between EFP2 and CCSD(T) or MP2 are small. The root-mean-square deviation (RMSD) between EFP2 and CCSD(T) potential energy curves for the sandwich, T-shaped, and hydrogen-bonded dimers is 0.49 kcal/mol, with a range from 0.31 kcal/mol (Bz−Py T3) to 0.66 kcal/mol ($(Py)_2$ S2). The maximum unsigned difference between EFP2 and CCSD(T) energies is 1.08 kcal/mol among sandwich dimers ($(Py)_2$ S2), while it is 1.97 among T-shaped dimers (Bz−Py T1), for which EFP2 tends to predict a much more rapid increase in potential energy at short intermonomer separations than CCSD(T). The RMSD between the EFP2 and SCS-MP2 curves for the parallel displaced dimers is 0.52 kcal/mol, with a maximum unsigned difference of 1.31 kcal/mol (for both types of parallel displaced benzene dimers). On average, the EFP2 potential energy curves for all dimers examined differ from the corresponding high-level ab initio curves by just 0.50 kcal/mol. EFP2 also provides an energy decomposition that compares well with SAPT2 results, making it an attractive method for use with aromatic heterocycles.

Dispersion and Coulomb interactions are the principal attractive forces in the dimers studied. Even in the hydrogen-bonded pyridine dimer, which is expected to be stabilized primarily by Coulomb attraction, the exchange-repulsion is of a similar magnitude. A similar observation is made for the lowest energy structures found with Monte Carlo/simulated annealing. While both the Bz−Py and $(Py)_2$ EFP2 MC/SA minimum-energy geometries involve direct interaction between the negatively charged heteroatom of pyridine and the positive carbon backbone

of the other monomer, the exchange-repulsion exceeds (in the case of Bz−Py) or nearly exceeds (in the case of $(Py)_2$) the Coulomb attraction. An accurate depiction of dispersion energy is necessary to describe the binding of these dimers.

■ ASSOCIATED CONTENT

Supporting Information. Cartesian coordinates of the minimum energy benzene−pyridine and pyridine dimer structures, along with the coordinates and interaction energy components of several additional low-lying geometries found with EFP2 Monte Carlo/simulated annealing. This material is available free of charge via the Internet at http://pubs.acs.org..

■ ACKNOWLEDGMENT

This work was supported by a grant (to M.S.G.) from the Air Force Office of Scientific Research and by a NSF CAREER and ACS PRF grants (to L.V.S.). The authors are grateful to Ed Hohenstein and Professor David Sherrill for providing high-level ab initio data for the benzene and pyridine dimers. The authors also gratefully acknowledge Iowa State University and Purdue University.

■ REFERENCES

(1) Burley, S. K.; Petsko, G. A. *Science* **1985**, *229*, 23. Hunter, C. A.; Singh, J.; Thornton, J. M. *J. Mol. Biol.* **1991**, *218*, 837.
(2) Saenger, W. *Principles of Nucleic Acid Structure*; Springer-Verlag: New York, 1984.
(3) Lerman, L. S. *J. Mol. Biol.* **1961**, *3*, 18. Brana, M. F.; Cacho, M.; Gradillas, A.; Pascual-Teresa, B.; Ramos, A. *Curr. Pharm. Des.* **2001**, *7*, 1745.
(4) Gordon, M. S.; Freitag, M. A.; Bandyopadhyay, P.; Jensen, J. H.; Kairys, V.; Stevents, W. J. *J. Phys. Chem. A* **2001**, *105*, 293. Jensen, J. H.; Gordon, M. S. *Mol. Phys.* **1996**, *89*, 1313.
(5) Slipchenko, L. V.; Gordon, M. S. *J. Comput. Chem.* **2007**, *28*, 276.
(6) Gordon, M. S.; Slipchenko, L. V.; Li, H.; Jensen, J. H. *Annu. Rep. Comp. Chem.* **2007**, *3*, 177.
(7) Smith, T.; Slipchenko, L. V.; Gordon, M. S. *J. Phys. Chem. A* **2008**, *112*, 5286.
(8) Raghavachari, K.; Trucks, G. W.; Pople, J. A.; Head-Gordon, M. *Chem. Phys. Lett.* **1989**, *157*, 479.
(9) Hohenstein, E. G.; Sherrill, C D. *J. Phys. Chem. A* **2009**, *113*, 878.
(10) Piacenza, M; Grimme, S. *ChemPhysChem* **2005**, *6*, 1554.
(11) Mishra, B. K.; Sathyamurthy, N. *J. Phys. Chem. A* **2005**, *109*, 6.
(12) Möller, C; Plesset, M. S. *Phys. Rev.* **1934**, *46*, 618.
(13) McLean, A. D.; Chandler, G. S. *J. Chem. Phys.* **1980**, *72*, 5639.
(14) Schmidt, M. W.; Baldridge, K. K.; Boatz, J. A.; Elbert, S. T.; Gordon, M. S.; Jensen, J. H.; Koseki, S.; Matsunaga, N.; Nguyen, K. A.; Su, S. J.; Windus, T. L.; Dupuis, M.; Montgomery, J. A. *J. Comput. Chem.* **1993**, *14*, 1347.
(15) Stone, A. J. *The Theory of Intermolecular Forces*: Oxford University Press: Oxford, U.K., 1996.
(16) Stone, A. J. *J. Chem. Theory Comput.* **2005**, *1*, 1128.
(17) Jenson, J. H.; Gordon, M. S. *Mol. Phys.* **1996**, *89*, 1313.
(18) Adamovic, I.; Gordon, M. S. *Mol. Phys.* **2005**, *103*, 379. Amos, R. D.; Handy, N. C.; Knowles, P. J.; Rice, J. E.; Stone, A. J. *J. Phys. Chem.* **1985**, *89*, 2186.
(19) Li, H.; Gordon, M. S.; Jensen, J. H. *J. Chem. Phys.* **2006**, *124* 214108.
(20) Slipchenko, L. V.; Gordon, M. S. *Mol. Phys.* **2009**, *107*, 999.
(21) Gauss, J.; Stanton, J. F. *J. Phys. Chem. A* **2000**, *104*, 2865.
(22) Innes, K. K.; Ross, I. G.; Moomaw, W. R. *J. Mol. Spectrosc.* **1988**, *132*, 492.
(23) Podeszwa, R.; Bukowski, R.; Szalewicz, K. *J. Phys. Chem. A* **2006**, *110* (34), 10345.
(24) Dunning, T. H. *J. Chem. Phys.* **1989**, *90*, 1007. Kendall, R. A.; Dunning, T. H.; Harrison, R. J. *J. Chem. Phys.* **1992**, *96*, 6796.
(25) Haliker, A.; Klopper, W.; Helgaker, T.; Jorgensen, P.; Taylor, P. R. *J. Chem. Phys.* **1999**, *111*, 9157.
(26) Grimme, S. *J. Chem. Phys.* **2003**, *118*, 9095.
(27) Boys, S. F.; Bernardi, F. *Mol. Phys.* **1970**, *19*, 553.
(28) Jeziorski, B.; Moszynski, R.; Szalewicz, K. *Chem. Rev.* **1994**, *94*, 1887. Williams, H. L.; Szalewicz, K.; Jeziorski, B.; Moszynski, R.; Rybak, S. *J. Chem. Phys.* **1993**, *98*, 1279.
(29) Day, P. N.; Pachter, R.; Gordon, M. S.; Merrill, G. N. *J. Chem. Phys.* **2000**, *112*, 2063.
(30) Sinnokrot, M. O.; Sherrill, C. D. *J. Phys. Chem. A* **2004**, *108*, 10200. Sinnokrot, M. O.; Valeev, E. F.; Sherrill, C. D. *J. Am. Chem. Soc.* **2002**, *124*, 10887.